Proton Transfer Mediated by the Vibronic Coupling in Oxygen Core Ionized States of Glyoxalmonoxime Studied by Infrared−X-ray Pump−Probe Spectroscopy

V. C. Felicíssimo,[†,‡] F. F. Guimarães,*[,†,‡] A. Cesar,[‡] F. Gel'mukhanov,[†] and H. Ågren[†]

Theoretical Chemistry, Roslagstullsbacken 15, Royal Institute of Technology, S-106 91 Stockholm, Sweden, and Departamento de Química, Universidade Federal de Minas Gerais, Av. Antonio Carlos, 6627, CEP-31270-901, Belo Horizonte, Minas Gerais, Brazil

Received: August 4, 2006; In Final Form: September 26, 2006

The theory of IR−X-ray pump−probe spectroscopy beyond the Born−Oppenheimer approximation is developed and applied to the study of the dynamics of intramolecular proton transfer in glyoxalmonoxime leading to the formation of the tautomer 2-nitrosoethenol. Due to the IR pump pulses the molecule gains sufficient energy to promote a proton to a weakly bound well. A femtosecond X-ray pulse snapshots the wave packet route and, hence, the dynamics of the proton transfer. The glyoxalmonoxime molecule contains two chemically nonequivalent oxygen atoms that possess distinct roles in the hydrogen bond, a hydrogen donor and an acceptor. Core ionizations of these form two intersecting core-ionized states, the vibronic coupling between which along the OH stretching mode partially delocalizes the core hole, resulting in a hopping of the core hole from one site to another. This, in turn, affects the dynamics of the proton transfer in the core-ionized state. The quantum dynamical simulations of X-ray photoelectron spectra of glyoxalmonoxime driven by strong IR pulses demonstrate the general applicability of the technique for studies of intramolecular proton transfer in systems with vibronic coupling.

I. Introduction

X-ray science sheds light on the structure of molecules due high inherent spatial resolution. The monitoring of the molecular dynamics poses a great challenge for X-ray spectroscopy due to the large number of applications in different areas of fundamental science and technology. Nowadays we have the possibility at hand of monitoring femtosecond nuclear motion using X-ray pulses provided by high-harmonic generation,[1] which is one of several sources of ultrashort X-ray pulses that have been developed recently.[2−4] Conventional X-ray photoelectron spectroscopy (XPS)[5] gives rather restricted information about the nuclear dynamics because the photoionization happens in a quite narrow Franck−Condon region near the ground-state equilibrium. As demonstrated recently,[6−9] this difficulty can be overcome by the application of a strong infrared (IR) pulse, which prepares a coherent superposition of vibrational states or nuclear wave packet. The time-resolved XPS technique applied to such a prepared system gives a unique opportunity to explore the nuclear dynamics in ground and core-ionized states.

The basic physics underlying IR−X-ray pump−probe spectroscopy was exemplified in our previous study of the proton transfer in the water dimer.[6] In this Article we study the intramolecular dynamic of proton transfer in glyoxalmonoxime (GM) leading to the formation of the tautomer 2-nitrosoethenol (NE), as a representation of the approach to a more common and larger organic molecular system.

Glyoxalmonoxime contains two chemically nonequivalent oxygen atoms O_1 and O_2 that possess distinct roles in the hydrogen bond wherein O_1 is a hydrogen donor and O_2 is a hydrogen acceptor. The ionization of the 1s electron of the donor or acceptor oxygen of GM leads to the formation of two $^2A'$ core-ionized diabatic states that show a crossing of their potential curves along the OH stretching mode related to the intramolecular proton-transfer channel in glyoxalmonoxime. The vibronic coupling of these states of the same symmetry partially delocalizes core-holes and affects the dynamics of the proton transfer in the core-ionized state. Ordinary XPS technology is useless here because it maps the dynamics in the narrow Franck−Condon region near the equilibrium; however, a coherent IR field changes the situation qualitatively. Indeed, due to the IR pump the molecule gains sufficient energy to promote the proton to the weakly bound proton-transfer well, which is 0.899 eV higher in energy than the global minimum. The IR induced nuclear wave packet performs back and forth routes from GM to NE wells. Now the probe X-ray pulse can excite the molecule in different regions of the core-ionized potential and can thereby monitor the dynamics of the proton-transfer accompanied by the vibronic coupling.

The aim of the present article is to theoretically investigate the IR−X-ray pump−probe spectroscopy of the intramolecular proton transfer in glyoxalmonoxime, the dynamics of which is accompanied by the vibronic coupling of intersecting core-ionized states. An unusual feature of the studied system is that, compared to the common situation when the vibronic coupling localizes the core hole,[10,11] one here faces the opposite effect, namely, a partial delocalization of the core hole caused by the vibronic coupling. The vibronic coupling even results in a core hole hopping. This makes the physics rather intriguing because the interaction with light pulses is followed by the simultaneous action of the nuclear dynamics (proton transfer) and electronic dynamics (core hole hopping).

The outline of the paper goes as follows. We begin with the description of the model in section II. The theoretical machinery is described in section III. In section IV we outline the numerical

* Corresponding author. E-mail: viviane@theochem.kth.se.
† Royal Institute of Technology.
‡ Universidade Federal de Minas Gerais.

10.1021/jp065036d CCC: $33.50
Published on Web 11/09/2006

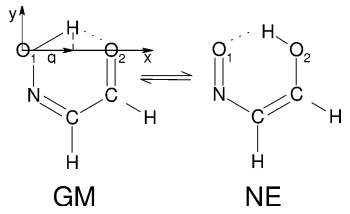

Figure 1. Glyoxalmonoxime (GM) and 2-nitrosoethenol (NE).

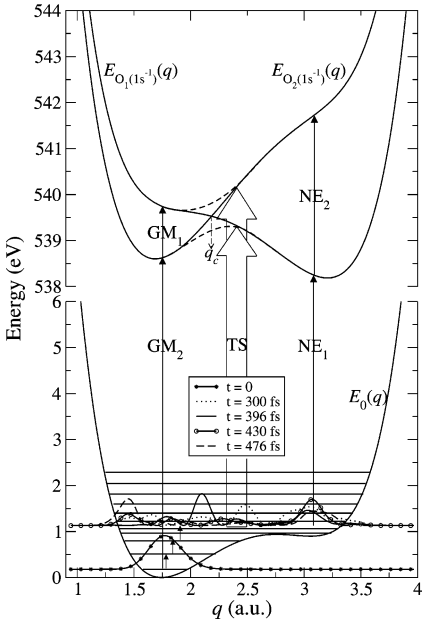

Figure 2. Potential energy curves of ground and core ionized states along a Cartesian coordinate q related to the proton-transfer channel. Dashed lines mark the adiabatic potentials $E_{\pm}(q)$ (21) for $\lambda q_c = 0.3$ eV. The minimum of $E_0(q)$ is situated at $q_0 = 1.74$ au. The diabatic potentials cross each other in the point $q_c = 2.18$ au.

procedure. The result of our wave packet simulations of the X-ray pump−probe spectra of the GM molecule are presented in section V. Section VI comprises a summary and attempts to offer a broader perspective of X-ray pump−probe technique in studies of the proton-transfer process accompanied by vibronic coupling.

II. Model

We consider ordinary OK X-ray photoionization of the GM molecule (Figure 1) as well as the photoionization of this molecule driven by a strong IR field in the ground electronic state. The interaction of the IR radiation with core-ionized molecules is absent in the studied case because of the delay of the short X-ray pulse relative to the IR pulse. Among the various conformations of the molecular structures of GM and NE tautomers,[12] we choose those presented in Figure 1 that make propitious the intramolecular hydrogen bond. To model the proton transfer that occurs along the x-axis (see Figure 2), we explore the one-dimensional dynamics of hydrogen along this axis with other nuclear degrees of freedom kept frozen. It is worth nothing that the IR field can excite also other vibrational modes that are close in frequency (such as the C−H mode). However, the excitation of these modes does not influence the proton transfer directly. This motivates us to use a simple 1D model that takes into account the major contribution to the effect. The potential energy curve $E_0(q)$ of the ground electronic state of the GM molecule along the nuclear coordinate q shows an asymmetric double well shape; see Figure 2. The global minimum of $E_0(q)$ occurs at $q_0 = 1.74$ au and corresponds to the tautomer GM. Here and below q is the projection of the O_1H bond on the x-axis, Figure 1. The increase of q up to 3.05 au leads to the intramolecular proton transfer in GM, resulting in the formation of the NE tautomer, which is 0.899 eV higher in energy. The NE well is quite shallow, being approximately 0.04 eV more stable than the transition state that occurs at $q = 2.75$ au.

When the intensity of IR field is zero, the XPS transitions occur from the bottom of the $E_0(q)$ well to the points of the vertical transitions GM_2 and GM_1. Thus without an IR field, one can expect to see two XPS bands GM_2 and GM_1 (Figure 2). The band GM_1 has a larger vibrational broadening than the GM_2 band due to the quasidissociative character of the $E_{O_1(1s)}(q)$ potential in the region of the vertical transition. A strong IR pulse changes qualitatively the X-ray photoelectron spectrum. Indeed, the coherent IR field excites higher vibrational levels and forms a nuclear wave packet that can approach the proton-transfer NE well ($q = 3.05$ au). The XPS transition from this well results in two new bands NE_1 and NE_2 (Figure 2).

Contrary to the ground-state potential $E_0(q)$, the diabatic $O_1(1\ s^{-1})$ and $O_2(1\ s^{-1})$ core ionized states possess asymmetric single well potentials $E_1(q) \equiv E_{O_1(1s^{-1})}(q)$ and $E_2(q) \equiv E_{O_2(1s^{-1})}(q)$ (Figure 2). In the diabatic $E_{O_2(1s^{-1})}$ potential, the minimum energy is located at $q = 1.69$ au, being rather close to the equilibrium $q_0 = 1.74$ au. On the other hand, the $E_{O_1(1s^{-1})}$ potential is deeper on 0.41 eV than the $O_2(1\ s^{-1})$ well and its minimum is shifted to the proton-transfer region at $q = 3.20$ au. The vertical $O_2(1\ s^{-1})$ and $O_1(1\ s^{-1})$ ionization potentials from the GM equilibrium position in the ground state are 538.61 and 539.72 eV, respectively. The $E_{O_1(1s^{-1})}$ and $E_{O_2(1s^{-1})}$ potentials show a crossing at $q_c = 2.18$ au. Vibronic coupling (VC) mixes these diabatic states. Let us explore in detail the role of the vibronic coupling on the dynamics of the proton transfer and on the X-ray pump−probe spectra.

III. Theoretical Methodology

A quantum dynamical treatment of the pump−probe experiment includes the preparation of the initial nuclear wave packet followed by the X-ray transition to the coupled core-ionized final states. We begin from the step of formation of the wave packet.

A. Ground-State Wave Packet Induced by the IR Field. The IR radiation creates a coherent superposition of the vibrational levels or wave packet $\phi(t)$ in the ground-state potential $E_0(q)$

$$|\phi(t)\rangle = \sum_{\nu} a_{\nu}(t)|\nu\rangle e^{-\imath\epsilon_{\nu}t}, \qquad \langle\phi(t)|\phi(t)\rangle = 1 \qquad (1)$$

where ϵ_ν and $|\nu\rangle$ are the vibrational energy and eigenvector of the ground electronic state, respectively. Thus the X-ray photoionization starts from the prepared initial molecular state $\Psi = \psi\phi(t)\exp(-\imath E_0 t)$. Here ψ is the electronic wave function of the ground state, and $E_0 = E_0(q_0)$ is the energy of the bottom of the ground-state potential that corresponds to the GM isomer, Figure 2. The nuclear wave packet (1) obeys the Schrödinger equation

$$\imath\frac{\partial}{\partial t}\phi(t) = H(t)\,\phi(t)$$
$$H(t) = H_0 - (\mathbf{d}\cdot\mathbf{E}_L(t))\cos(\omega_L t + \varphi_L) \qquad (2)$$

with the initial condition $|\phi(0)\rangle = |0\rangle$. Here $\mathbf{d} = \mathbf{d}_{00}(q)$ is the dipole moment of the ground electronic state; $\mathbf{E}_L(t)$, φ_L and ω_L

are the strength of electric field, phase and frequency of the IR field, respectively. In our model the nuclear Hamiltonian of the ground state is nothing other than the Hamiltonian of the hydrogen atom

$$H_0 = -\frac{1}{2m_H}\frac{d^2}{dq^2} + E_0(q) - E_0 \quad (3)$$

where m_H is the hydrogen mass. It is worth nothing that the reduced mass $m_H(M - m_H)/M$ is replaced by m_H because the ratio of hydrogen mass to the total molecular mass is small $m_H/M \approx 0.003$. We ignore the small lifetime broadening of the vibrational levels of the ground electronic state ($\Gamma_0^{-1} \gtrsim 1$ ps). This time is much longer than the delay time and duration of the X-ray pulse considered in this article. Let us note that the spatial phases $\mathbf{k}_L\cdot\mathbf{q}$ and $\mathbf{k}_X\cdot\mathbf{q}$ are ignored in the remaining part of the Article. The role of these phases can be important in some cases as was already discussed in ref 13.

B. Evolution of Nuclear Wave Packets on the Two Coupled Core Ionized States. In this section we explore the dynamics of the nuclear wave packet excited by weak X-ray radiation on the core ionized states. The ionization of one electron in $O_1(1s)$ or $O_2(1s)$ orbital of glyoxalmonoxime (Figure 1) generates respectively the diabatic electronic states $|\psi_1\rangle$ and $|\psi_2\rangle$, which show a crossing of their potential energy curves $E_{O_1(1s-1)} \equiv E_1(q)$ and $E_{O_2(1s-1)} \equiv E_2(q)$ at the nuclear coordinate $q = q_c$; see Figure 2. The total wave function of the core ionized states is written as

$$\Psi_c = (\psi_1\phi_1(t) + \psi_2\phi_2(t))e^{-\iota E_c t} \quad (4)$$

where E_c is defined as the lowest energy between the two core ionized potentials $E_1(q)$ and $E_2(q)$; ψ_1 and ψ_2 are the electronic time-independent wave functions of the core ionized states in the Born−Oppenheimer approximation. The nuclear wave packets ϕ_1 and ϕ_2 of the electronic states ψ_1 and ψ_2, respectively, form the two component nuclear wave packet of the core-ionized state

$$|\phi_c(t)\rangle = \begin{pmatrix} |\phi_1(t)\rangle \\ |\phi_2(t)\rangle \end{pmatrix} \quad (5)$$

which obeys the coupled equations

$$\iota\frac{\partial}{\partial t}\phi_1(t) = H_{11}\phi_1(t) + H_{12}\phi_2(t) + V_{10}(t)\phi(t)$$
$$\iota\frac{\partial}{\partial t}\phi_2(t) = H_{21}\phi_1(t) + H_{22}\phi_2(t) + V_{20}(t)\phi(t). \quad (6)$$

It is useful to write down the matrix representation of these equations

$$\iota\frac{\partial}{\partial t}\boldsymbol{\phi}_c(t) = \mathscr{H}\boldsymbol{\phi}_c(t) + \mathbf{V}(t)\,\phi(t)$$
$$\mathbf{V}(t) = \begin{pmatrix} V_{10}(t) \\ V_{20}(t) \end{pmatrix}$$
$$\boldsymbol{\phi}_c(t) = \begin{pmatrix} \phi_1(t) \\ \phi_2(t) \end{pmatrix} \quad (7)$$

where $V_{n0}(t) = -(\mathbf{D}_{n0}\cdot\mathbf{E}_X(t))\cos(\omega_X t)\exp(\iota(\epsilon + E_c - E_0)t)$ is the matrix element of the interaction between the molecule and the X-ray field; ϵ is the energy of the photoelectron; ω_X, $\mathbf{e}_X$, and $E_X(t)$ are respectively the frequency, polarization vector and the electric field of the X-ray field; $\mathbf{E}_X(t) = \mathbf{e}_X E_X(t)$; and $\mathbf{D}_{n0}$ is the transition dipole moment of the core ionization of the oxygen $n = 1, 2$.

Equation 7 describes the dynamics of the wave packet $\phi_c(t)$ in the two coupled core ionized states with the nuclear Hamiltonian

$$\mathscr{H} = \begin{pmatrix} H_{11} & H_{12} \\ H_{21} & H_{22} \end{pmatrix} \quad (8)$$

Here the diagonal terms

$$H_{nn} = -\frac{1}{2m_H}\frac{d^2}{dq^2} + E_n(q) - E_c, \qquad n = 1, 2 \quad (9)$$

describe the independent nuclear motion in the diabatic potentials $E_n(q) = \langle\psi_n|H_{el}|\psi_n\rangle$ of the core-ionized electronic states ψ_n.

A special comment deserves the off-diagonal terms, H_{nm}, which are responsible for nonadibatic transitions. Two different approaches are used to deal with such a problem, namely, the differential form of the VC operator

$$H_{12} = -H_{21} = -\frac{1}{2m_H}\left[2C_{12}(q)\frac{d}{dq} + \left(\frac{dC_{12}(q)}{dq}\right)\right]$$
$$C_{12}(q) = \left\langle\psi_1(r,q)\left|\frac{d}{dq}\right|\psi_2(r,q)\right\rangle \quad (10)$$

and the linear scalar Herzberg−Teller representation[14]

$$H_{12} = H_{21} = \lambda q \quad (11)$$

that is equivalent to the linear coupling model of Cederbaum et al.,[10] for constant λ parameter. This simple model is quite useful for treating nonadiabatic cases where small molecular distortion motions are involved close to a reference molecular geometry, usually the electronic molecular ground-state geometry, and the scalar or Herzberg−Teller (HT) representation. These representations differ from each other in the electronic wave functions that depend parametrically on the nuclear coordinates in the former case, whereas the electronic wave functions are taken in a fixed nuclear geometry in the second case.[15] Both approaches should give the same result if the total function is expanded over a complete electronic basis set. We use the scalar form of the VC operator (11) because the HT representation is preferable from the numerical point of view.[10] The only exception is section VC.2, where we model the vibronic coupling H_{12} by a Gaussian.

C. Probability of X-ray Photoionization of Molecules Driven by a Strong IR Field. One can solve directly the coupled equations (6) to find the photoionization cross section.[16] However, this numerical scheme is rather expensive, because to obtain a spectrum we need to solve equations for each value of the photoelectron energy ϵ. We follow instead an alternative technique based on the fact that the photoionization probability is the norm of the core ionized wave packet in the frequency domain

$$P(\Omega) = \langle\boldsymbol{\varphi}_c(\Omega)|\boldsymbol{\varphi}_c(\Omega)\rangle = \langle\varphi_1(\Omega)|\varphi_1(\Omega)\rangle + \langle\varphi_2(\Omega)|\varphi_2(\Omega)\rangle \quad (12)$$

This and the equations below generalize our previous results obtained for nuclear dynamics in a single excited electronic state.[6,8,17] The Fourier transform of eq 7 gives a two-component wave packet of the core hole state in the frequency domain

$$|\varphi_n(\Omega)\rangle = \int_{\infty}^{-\infty} dt\, e^{-\iota\Omega t} E_X(t)|\varphi_n(t)\rangle \qquad n = 1, 2 \quad (13)$$

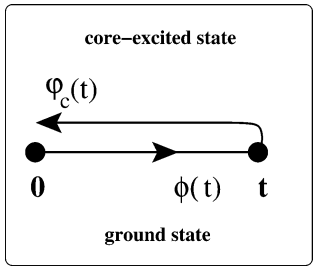

Figure 3. Time loop used for the calculation of the wave packet in the core excited potential surface. IR field creates the nuclear wave packet $\phi(t)$ in the ground-state well, which evolves from the moment 0 up to t. At the instant t, the X-ray field promotes the ground-state wave packet $\phi(t)$ in two coupled core-ionized states. The wave packets $\varphi_1(t)$ and $\varphi_2(t)$ evolve in the core-ionized states in the inverse direction from moment t up to 0.

which is the Fourier transform of the new wave packet

$$\boldsymbol{\varphi}_c(t) = \begin{pmatrix}\varphi_1(t)\\ \varphi_2(t)\end{pmatrix} = e^{\iota\mathscr{H}t}\boldsymbol{\zeta}\phi(t)$$
$$\boldsymbol{\zeta} = \begin{pmatrix}\zeta_1\\ \zeta_2\end{pmatrix}$$
$$\zeta_n = \frac{1}{2}(\mathbf{D}_{n0}\cdot\mathbf{e}_X) \qquad (14)$$

Here $\Omega = \mathrm{BE} - I_{1s}$ is the relative binding energy ($\mathrm{BE} = \omega_X - \epsilon$), where $I_{1s} = E_c - E_0$ is the smallest adiabatic core ionization potential (between the wells 1 and 2); the lifetime broadening of the core-ionized state $\Gamma_c = 0$ is neglected here and below.

Contrary to the wave packet $\phi_c(t)$ (7) the wave packet $\varphi_c(t)$ does not depend on the photoelectron energy ϵ. Due to such an essential advantage we use $\varphi_c(t)$ instead of $\phi_c(t)$ in the numerical simulations. The calculation of $\varphi_c(t)$ is performed along the contour (Figure 3) where the ground-state wave packet $\phi(t)$ (2) evolves from the moment 0 up to t. The X-ray field promotes $\phi(t)$ at the instant t in the two coupled core-ionized states where the newly formed wave packet $\varphi_c(t)$ evolves in the inverse direction from moment t up to 0. The dynamics in the inverse direction is seen from the fact that the wave packet $\varphi_c(t) \equiv \varphi_c(0,t)$ is the solution of the Schrödinger equation

$$\iota\frac{\partial}{\partial\tau}\boldsymbol{\varphi}_c(\tau,t) = \mathscr{H}\varphi_c(\tau,t) \qquad (15)$$

from $\tau = t$ till 0 with the initial condition $\varphi_c(t,t) = \zeta\phi(t)$.

Equation 12 shows that the total XPS probability is the sum of the partial probabilities $P_1(\Omega) = \langle\varphi_1(\Omega)|\varphi_1(\Omega)\rangle$ and $P_2(\Omega) = \langle\varphi_2(\Omega)|\varphi_2(\Omega)\rangle$ related to the two photoioization channels $O_1(1\ s^{-1})$ and $O_2(1\ s^{-1})$, respectively.

IV. Details of Numerical Simulations

A. Computational Aspects. The 1D-simulations of X-ray pump−probe spectra are performed for the GM molecule depicted in Figure 1. As already mentioned, the calculations are done along the nuclear coordinate q, which is the projection of the O_1H bond on the x-axis. Other nuclear degrees of freedom are frozen.

The diabatic potential energy curves of the ground and core ionized states (Figure 2) and the Cartesian components of the permanent dipole moment of the ground state (Figure 4) are computed point to point using density functional theory (DFT/B3LYP)[18] as implemented in the GAMESS program.[19] The 6-311++G** basis set[20] was employed to perform all calculations. The simulations give the following values for the adiabatic

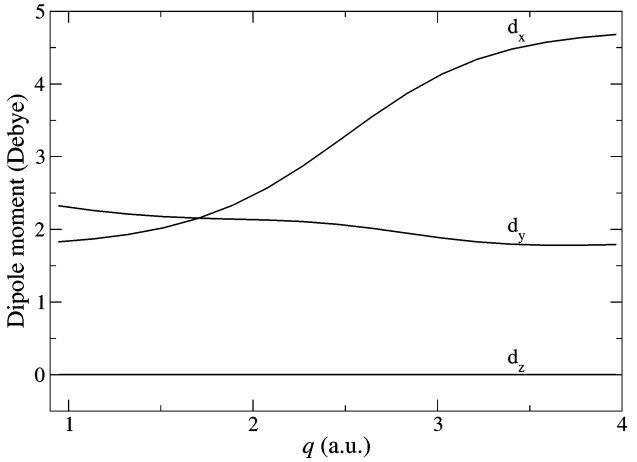

Figure 4. Dependence of the permanent dipole moment components $d_m(q)$ of the GM molecule in the ground state on the nuclear coordinate q.

ionization potentials of the oxygen atoms: O_1 ($I_{1s}^{(1)} = 538.19$ eV) and O_2 ($I_{1s}^{(2)} = 538.60$ eV). The XPS spectra are computed versus the binding energy ($\mathrm{BE} = \omega_X - \epsilon$), $\Omega = \mathrm{BE} - I_{1s}^{(1)}$ with respect to the smallest adiabatic ionization potential, 538.19 eV.

The simulations of spectra are divided in four blocks: (1) calculation of the nuclear wave packet (WP) $\phi(t)$ driven by the IR pulse in the ground electronic state, solving numerically the Schrödinger eq 2, (2) evaluation of the two-component nuclear wave packet $\varphi_c(t)$ (14) in the two coupled core-excited states with the Hamiltonian (8), (3) Fourier transform, $\varphi_c(\Omega)$ (13), of the wave packet $\varphi_c(t)$, and (4) calculation of the norm $\langle\varphi_c(\Omega)|\varphi_c(\Omega)\rangle$, which is nothing other than the probability of X-ray ionization $P(\Omega)$ (12).

The IR−X-ray pump probe spectra are computed using the wave packet techniques implemented in the e*SP* ec program.[21] A second-order differential scheme is used in the calculations of ground and core ionized wave packets with a time step of 5×10^{-5} fs along the nuclear coordinate q from 0.95 to 3.97 au using a spatial discretization of 310 points.

The lifetime broadenings of the ground-state vibrational levels as well as of the core-ionized state are neglected in calculations due to rather short IR and X-ray pulses.

B. Shape and Parameters of the Light Pulses. The following relation between parameters in atomic units and in SI units are used in the calculations: dE (au) = d (debye) × $\sqrt{I(\mathrm{W/cm^2})} \times 2.1132 \times 10^{-9}$ au, Ωt (au) = Ω (au) × t (fs) × 41.3417. Here $I = c\epsilon_0|E(t)|^2/2$ is the intensity of radiation. The temporal shape of the IR ($\alpha = L$) and X-ray ($\alpha = X$) pulses are modeled in the calculations by a gaussian

$$I_\alpha \exp\left[-\left(\frac{t - t_\alpha}{\bar{\tau}_\alpha}\right)^2\right], \qquad \bar{\tau}_\alpha = \frac{\tau_\alpha}{\sqrt{\ln 2}} \qquad (16)$$

where τ_α is the half width at half-maximum (HWHM) and t_α is the peak position of the IR or X-ray pulses.

The parameters of the IR pulse used to generate the ground-state wave packet are $t_L = 200$ fs, $\tau_L = 10$ fs, $I_L = 2.3 \times 10^{14}$ W/cm^2, and $\varphi_L = 0.53$ rad. The IR field is assumed to be in resonance with the first vibrational transition $\omega_L = \omega_{10} = 0.33$ eV. The phase ($\varphi_L = 0.53$ rad) was adjusted to get the maximum intensity of the few-cycle IR pulse at the instant $t_L = 200$ fs. We use a short IR pulse, $\tau_L = 10$ fs, which allows us to overcome the anharmonicity of the higher vibrational states

which should to be excited to reach the proton-transfer region (see Figure 2).

To make snapshots of the ground-state wave packet $\phi(t)$, we use a rather short X-ray probe pulse with the duration $\tau_X = 4$ fs (except Figures 7 and 9). The XPS spectra are calculated for different delay times between X-ray and IR pulses, $\Delta t = 100$, 196, 230 and 276 fs. The IR pulse has time to leave the system for such delays. Due to this the spectral composition of the wave packet $\phi(t)$ is the same for all these delays.

C. Molecular Orientation. The molecular orientation deserves special comment. Here we study the XPS spectra with the O_1-O_2 bond aligned parallel to the polarization vector of the IR field, $\mathbf{e}_L$. X-ray photoelectron spectra of fixed-in-space molecules can be measured in electron−ion coincidence experiments applied to randomly oriented molecules.[22,23] Let us mention also the possibility of alignment or orientation of the molecules by a strong IR fields.[24]

However, our analysis can be useful also in ordinary XPS measurements with randomly oriented molecules. The reason for this is an asymmetry of the studied molecule and, hence, strong anisotropy of its interaction with the radiation. The interaction of the IR radiation with the vibrational modes of GM depends on the magnitude of the variation of the permanent dipole moment, $\mathbf{d}(q)$, along the nuclear coordinate q. Indeed, the amplitude of the vibrational transitions in the IR field

$$\langle 0|\mathbf{e}_L \cdot \mathbf{d}(q)|\nu\rangle \tag{17}$$

is equal to zero when $\mathbf{d}(q) = \text{const}$. Here $\mathbf{e}_L$ is the polarization vector of the IR radiation. The q dependence of the Cartesian components of the total permanent dipole moment of the ground-state GM are shown in Figure 4. One can see in Figure 4 that the d_z component does not depend on q, and d_y shows a very small q dependence compared with the d_x component. Thus, mainly the molecules with the O_1-O_2 bond aligned parallel to $\mathbf{e}_L$ interact with the IR radiation. This motivates us to explore the X-ray + IR pump−probe spectra for such a parallel alignment of the molecules.

V. Results

A. Potential Energy Curves and the Proton Transfer. Figure 2 shows qualitatively different potentials for ground $E_0(q)$ and core ionized states $E_{O_1(1s^{-1})}(q)$ and $E_{O_2(1s^{-1})}(q)$. When the diabatic potentials $E_{O_1(1s^{-1})}$ and $E_{O_2(1s^{-1})}$ interact with each other via the vibronic coupling, the crossing is avoided, leading to the formation of the adiabatic potentials represented by $E_-(q)$ (double well potential) and $E_+(q)$ (single well potential), as shown by dashed line in Figure 2. As is well-known, the adiabatic states are also vibronically coupled.

The core hole "sits" on the same oxygen during the proton transfer if the vibronic coupling of core ionized states $O_1(1\ s^{-1})$ and $O_2(1\ s^{-1})$ is absent. This means that during wave packet evolution the following interconversion reactions $GM[O_1(1\ s^{-1})] \rightleftharpoons NE[O_1(1\ s^{-1})]$ or $GM[O_2(1\ s^{-1})] \rightleftharpoons NE[O_2(1\ s^{-1})]$ takes place. Vibronic coupling of the $O_1(1\ s^{-1})$ and $O_2(1\ s^{-1})$ states allows the hopping of core-hole into another atom, leading to the switch-back interconversion reactions $GM[O_1(1\ s^{-1})] \rightleftharpoons NE[O_2(1\ s^{-1})]$ and $GM[O_2(1\ s^{-1})] \rightleftharpoons NE[O_1(1\ s^{-1})]$ caused by a proton transfer.

B. Orbital View on the Avoided Crossing. The Born−Oppenheimer approximation breaks down near the point q_c where the potential surfaces cross each other. The role of the VC becomes here important. To find electronic states where the role of the VC is large, we need to perform rather expensive simulations of different excited states. However, one can get information about a crossing of different states making use of a simple analysis of the q dependence of one-electron energies $\epsilon_i(q)$ obtained from the ground-state calculation. Such an approximate technique is based on Koopmans' theorem[25] which says that the energy of the ionized state $|i^{-1}\rangle$ is

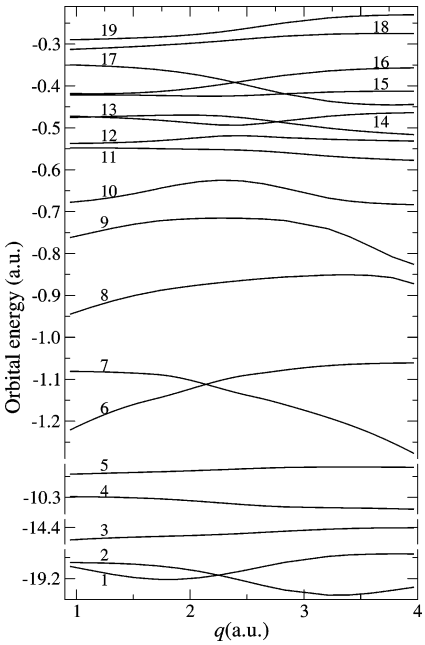

Figure 5. Energies of occupied molecular orbitals $\epsilon_i(q)$ versus the nuclear coordinate q.

$$E_i(q) \approx E_0(q) - \epsilon_i(q) \tag{18}$$

where $\epsilon_i(q)$ is the energy of the ith molecular orbital (MO). This equation allows us to write down the condition of the crossing of potential surfaces $E_i(q)$ and $E_j(q)$

$$\epsilon_i(q_c) = \epsilon_j(q_c) \tag{19}$$

Thus the shapes of the potentials $E_i(q)$ and $E_j(q)$ are defined by the ground-state potential $E_0(q)$ as well as by the one-electron energies $\epsilon_i(q)$ and $\epsilon_j(q)$. The q dependence of one-electron energies and the contour plots of corresponding MOs are depicted in Figures 5 and 6, respectively.

Let us first consider the ionization of the 1s levels 1 and 2 that are localized on the O_1 and O_2 atoms, respectively. The q dependences of $\epsilon_1(q)$ and $\epsilon_2(q)$ (Figure 5) and eq 18 explain the shapes of the potentials of core excited states (Figure 2). The crossing point 2.25 au given by the Koopmans' approximation (19) is rather close to the strict value $q_c = 2.18$ au.

According to Figure 5 one can also expect the crossing of the potentials and, hence the VC, near $q = 2.14$ au for $|6^{-1}\rangle$ and $|7^{-1}\rangle$ ionized states, near $q = 2.76$ au for $|13^{-1}\rangle$ and $|14^{-1}\rangle$ states, near $q = 2.83$ au for $|15^{-1}\rangle$ and $|17^{-1}\rangle$ states, and near $q = 2.39$ au for $|16^{-1}\rangle$ and $|17^{-1}\rangle$ states.

Figure 5 shows that the energies of the sixth and seventh orbitals have the strongest dependence on q. These orbitals are formed by the ligand combination of the 2s atomic orbitals localized on the NO and CO groups, respectively, as shown in Figure 6. Although the proton is being transferred from the GM to NE structures, the single and double characters of the NO and CO bonds, respectively, are inverted. This drastic change on the molecular skeleton during the intramolecular proton-transfer reaction is probably the main reason of large gradients $\partial\epsilon_6(q)/\partial q$ and $\partial\epsilon_7(q)/\partial q$ near the crossing point. It is reasonable

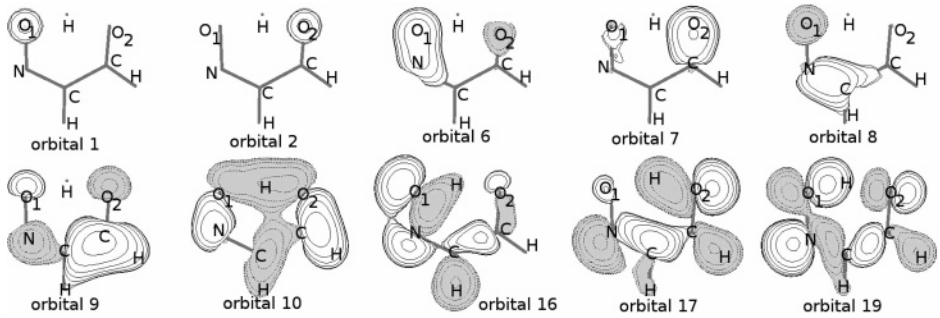

Figure 6. Occupied molecular orbitals of the GM molecule.

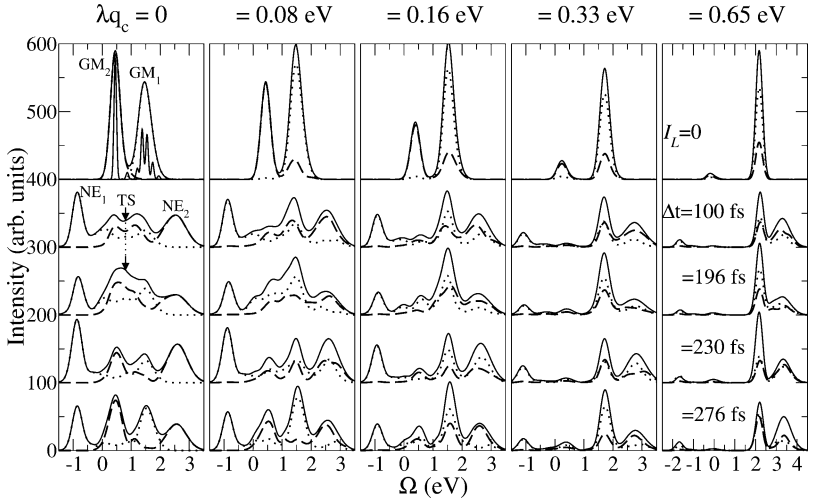

Figure 7. IR−X-ray pump−probe spectra of the oriented GM molecule ($\vec{\mathbf{e}}_L \parallel x$) for different values of the vibronic coupling constant λ and different delay times $\Delta t = t_X - t_L$ between X-ray and IR pulses. The crossing point of the diabatic $O_1(1\ s^{-1})$ and $O_2(1\ s^{-1})$ potentials is $q_c = 2.18$ au. Upper panels show XPS profiles for $I_L = 0$, and the lower panels show the spectra of molecules driven by the IR field. The parameters of the IR pulse are $I_L = 2.3 \times 10^{14}$ W/cm^2, $t_L = 200$ fs, $\tau_L = 10$ fs, $\varphi_L = 0.53$ rad and $\omega_L = \omega_{10} = 0.33$ eV. The duration of the X-ray pulse is $\tau_X = 4$ fs. The full lines show the total photoionization probabilities. The dotted and dashed curves are the partial photoionization probabilities $P_1(\Omega)$ and $P_2(\Omega)$, respectively, as explained in section III.C. The vibrationally resolved XPS profile depicted in the left upper panel was calculated for longer X-ray pulse, $\tau_X = 15$ fs.

to assume a similar strong q dependence of the corresponding MOs. Probably these molecular orbitals give major contribution in the VC constant C_{12} (10) and, hence, λ (11).

C. X-ray Photoionization without IR Field: Bright and Dark States. Let us begin with the case when IR radiation is absent, $I_L = 0$. The ordinary XPS spectra are depicted in the upper panels of Figure 7 for different VC constants, λ. As already explained in section II, the XPS profile consists of narrow GM_2 and wider GM_1 bands (Figure 7), which correspond to the vertical transitions from the bottom of the ground-state potential ($q_0 = 1.74$) to the wells $E_1(q) = E_{O_1(1s^{-1})}(q)$ and $E_2(q) = E_{O_2(1s^{-1})}(q)$, respectively. We do not see any fine structure because the X-ray pulse is short, $\tau_X = 4$ fs. However, the vibrational structure of both GM_1 and GM_2 bands becomes resolved when the duration of the pulse is longer than the vibrational period (see left upper panel in Figure 7). Now the GM_2 band consists of strong 0−0 line and very weak 0−1 vibrational transitions. It is because the minimum position (1.69 au) of the $E_{O_2(1s^{-1})}(q)$ well is rather close to the equilibrium $q_0 = 1.74$ au. The GM_1 band has a richer vibrational structure due to large displacement of the $E_{O_1(1s^{-1})}(q)$ well from the equilibrium. The vibrational frequency of the GM_1 band is essentially smaller than in the GM_2 well, because the $E_{O_1(1s^{-1})}(q)$ potential is quite shallow in the Franck−Condon region.

The upper panels of Figure 7 show the suppression of the GM_2 band when the coupling constant grows. This effect is seen clearly in the XPS spectra with and without an IR field. To understand the origin of this phenomenon, we analyze XPS spectra for fixed nuclear configuration. The vibronic coupling $H_{12} = \lambda q$ mixes two diabatic electronic states ψ_1 and ψ_2 and results in adiabatic states

$$\psi_+ = \psi_1 \sin\beta + \psi_2 \cos\beta \qquad \psi_- = \psi_1 \cos\beta - \psi_2 \sin\beta \tag{20}$$

with the energies

$$E_\pm(q) = \frac{1}{2}[E_1(q) + E_2(q) \pm \sqrt{(E_2(q) - E_1(q))^2 + 4H_{12}{}^2}] \tag{21}$$

Such a mixing delocalizes core holes and results in the following expression for the dipole moment $\langle\psi_\pm|d|\psi_0\rangle = d(\cos\beta \pm \sin\beta)$ of transition in these new states

$$d_\pm = \frac{d}{\sqrt{2}}\left(\sqrt{1 \mp \frac{1}{1+\zeta^2}} \pm \frac{\lambda}{|\lambda|}\sqrt{1 \pm \frac{1}{1+\zeta^2}}\right)$$
$$\zeta = \tan 2\beta = \frac{2\lambda q}{\Delta(q)} \tag{22}$$

where $\Delta(q) = |E_2(q) - E_1(q)|$ is the spacing between potentials $E_2(q)$ and $E_1(q)$. The vertical transitions to the ψ_+ and ψ_- states form the GM_1 and GM_2 bands, respectively. Let us remind that in high-energy region the transition dipole moments of core-ionization of both oxygens are the same, $d_1 = d_2 = d$, when the energy of photoelectron is rather high. The gap between the adiabatic potentials at the crossing point q_c (where $E_2(q_c)$

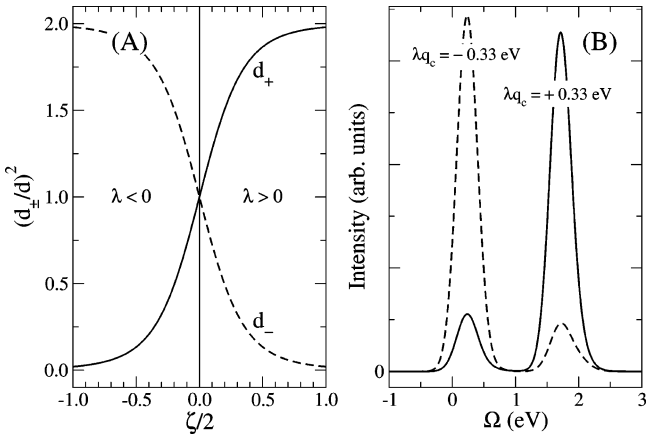

Figure 8. (A) XPS intensities $(d_\pm/d)^2$ (22) versus the coupling strength, $\zeta/2 = \lambda q/\Delta(q)$. $\Delta(q_0) = 1.02$ eV. (B) XPS spectra for positive and negative VC strengths (no IR field). Other parameters are the same as in Figure 7.

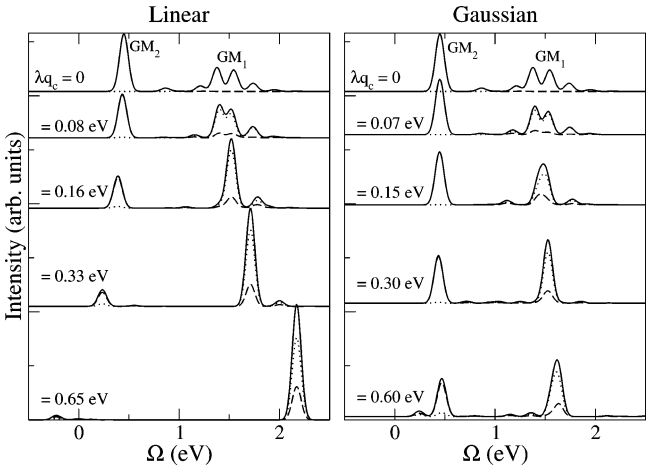

Figure 9. XPS profiles of the GM molecule without IR field for linear (11) and Gaussian (24) VC models. $a = 0.24$ au. $\tau_X = 15$ fs.

$= E_1(q_c)$) gives the VC parameter

$$2|\lambda|q_c = E_+(q_c) - E_-(q_c) \tag{23}$$

The intensities $(d_+/d)^2$ and $(d_-/d)^2$ (Figure 8A) display qualitatively different dependencies on the coupling strength λq_c due to the constructive and destructive interference of localized core-hole states (20) caused by VC. When $\lambda > 0$, one can see the quenching of the "dark" ψ_- state and the enhancement of the XPS intensity of the "bright" state ψ_+ with the increase of λ. According to eq 22 the dark and bright states are interchanged if the sign of VC is unversed $\lambda < 0$. We see this clearly from our rough estimate (22) (Figure 8A) as well as from strict simulations (Figure 8B).

Gaussian Model of Vibronic Coupling. In our simulations we follow the conventional VC model[10] with linear coupling $H_{12} = \lambda q$ (11) assuming λ to be constant. However, the vibronic coupling can have stronger dependence on q. To mimic such a possibility, we model the VC interaction by a Gaussian[26]

$$H_{12} = \lambda q_c e^{-(q-q_c)^2/a^2} \tag{24}$$

Figure 9 displays the XPS profile of the GM molecule without IR field. To resolve the vibrational structure, we use a rather long X-ray pulse, $\tau_X = 15$ fs. First of all, one can see that the quenching of the GM_2 band in the Gaussian model starts for rather high coupling parameters λq_c as compared with the linear model. The reason for this is the strong quenching of the Gaussian coupling (24) on the way from the crossing point, q_c. Because the manifestation of the VC is stronger in the linear coupling model (11) we see that the GM_1 and GM_2 bands separate when the linear coupling grows. This is in agreement with the expression (21) for the spacing between these bands, $E_+(q) - E_-(q)$. Another interesting result is that the GM_1 vibrational profile collapses to the single 0−0 line for large λq_c. This is because the miminum of the adiabatic potential $E_+(q)$ approaches the minimum of the ground-state well ($q_0 = 1.74$ au), when the coupling is large.

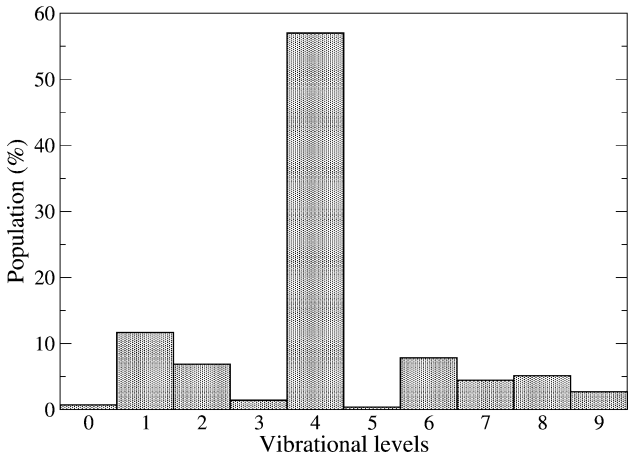

Figure 10. Populations of vibrational levels ($\nu = 0, 1, 2, ..., 9$) of the ground state of the GM molecule after the IR pulse left the system. Other parameters are the same as in Figure 7.

D. X-ray Photoionization in the Field of Strong IR Pulses. A short IR pulse ($\tau_L = 10$ fs) with the intensity $I_L = 2.3 \times 10^{14}$ W/cm^2 creates a ground-state wave packet $\phi(t)$. When the IR pulse leaves the system, the populations of vibrational levels cease to depend on the time and the main contribution (57%) in $\phi(t)$ gives the vibrational level $\nu = 4$ (Figure 10). The energy stored in this wave packet ($\langle\phi(t)|H_0|\phi(t)\rangle = 1.13$ eV) allows the molecule to reach the region of proton transfer in the ground-state potential (see Figure 2). Thus the GM molecule gains sufficient energy to reach the weakly bound proton-transfer well, where the NE tautomer is formed. It is interesting to note that level 4 can be populated due to a direct transition $0 \rightarrow 4$, which has a large transition dipole moment because of the strong anharmonicity of the ground-state potential near this level (see Figure 2). The simulations show that the direct population of the level $\nu = 4$ is about 25−80% for $\tau_L = 300-2640$ fs and $I_L = 2.3 \times 10^{14}$ W/cm^2.

The dynamics of $\phi(t)$ (Figure 11) shows that for the times $t \gtrsim t_L = 200$ fs the wave packet becomes delocalized and perform back and forth oscillations in the ground-state well. During these oscillations $\phi(t)$ periodically approaches the NE well ($q = 3.05$ au). The vertical transitions from this well form two new XPS bands at −0.84 eV (NE_1) and 2.63 eV (NE_2), which are attributed to the proton transfer in the GM molecule (see Figure 7). On the way from the shallow NE well to the GM well the wave packet crosses the transition state. X-ray photoionization at the TS region occurs at the spectral region between the bands GM_1 and GM_2 (Figure 7).

Referring back to the dependence of the XPS profile on the VC strength (Figure 7), we see that the intensity ratios of the peaks NE_1 and NE_2 display trends similar to those of the peaks GM_2 and GM_1. The formal reason for this is that the resonances NE_2 and NE_1 correspond to the ψ_+ and ψ_- solutions (22), respectively. One can see that, contrary to the peak GM_2, the

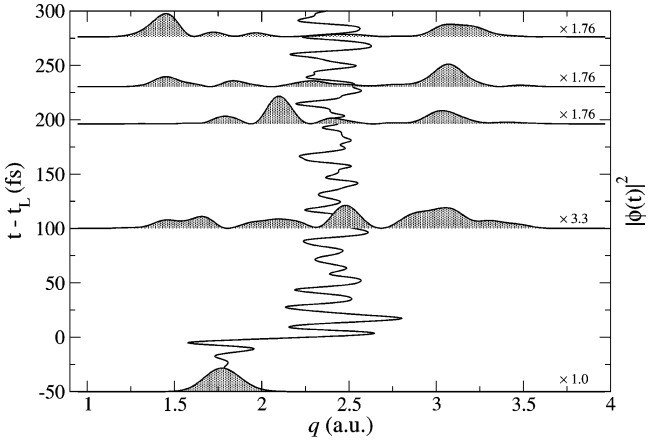

Figure 11. Squared wave packet $|\phi(t)|^2$ and its trajectory, $\langle\phi(t)|q|\phi(t)\rangle$ (solid line), versus the time. Other parameters are the same as in Figure 7.

peak NE_1 starts to become quenched for larger VC strengths. The reason for this is the larger gap between $E_{O_2(1s^{-1})}(q)$ and $E_{O_1(1s^{-1})}(q)$ potentials near $q = 3.05$ au than near the equilibrium $q = 1.74$ au. Indeed, the larger gap $\Delta(q)$ needs larger λ to get the same value of ζ and, hence, the same XPS intensity (see eq 22).

To see the role of the dynamics of the wave packet $\phi(t)$, we computed the XPS spectra for different delay times of the X-ray pulse, Δt (Figure 7). It is worth noting that the XPS spectra do not depend on Δt if the IR field is incoherent, except for the trivial time dependence due to the vibrational relaxation. Let us discuss the case with $\lambda = 0$. One can see comparable intensities of $GM_{1,2}$ and $NE_{1,2}$ bands for $\Delta t = 100$ fs due to the strong delocalization of the wave packet (Figure 11). At $\Delta t = 196$ fs the maximum of the wave packet approaches the crossing point ($q_c = 2.18$ au), which results in an enhancement of the TS band. Later on ($\Delta t = 230$ fs), the wave packet is localized in the NE well and the $NE_{1,2}$ bands become more intense. The picture is inverted (the $GM_{1,2}$ bands are larger) at the instant $\Delta t = 276$ fs when the maximum of $|\phi(t)|^2$ is shifted to the GM well.

Referring to Figure 11, one can realize the bottleneck of our study: We see that the wave packet is considerably delocalized. Such a delocalization restricts the spatial resolution of this technique, because it does not allow excitation of the nuclear subsystem explicitly in a desired point q. This means that the shaping of the narrow nuclear wave packet deserves special attention, a problem well worth considering. The main reason for delocalization of the wave packet in our case is known namely by the rather poor spectral composition of the wave. Indeed, the vibrational level $\nu = 4$ contributes almost 60% in $\phi(t)$ (Figure 10). We got stronger localization of $\phi(t)$ in the water dimer[6] by exciting simultaneously many vibrational levels.

To conclude this section, one can say that a VC constant λq_c larger than 0.1 eV is an apparent exaggeration for core ionization due to small overlap of 1s functions localized on different oxygen atoms. However, we included in our analysis also large λ, keeping in mind the proton transfer that can occur also under photoionization of valence molecular orbitals where the coupling is stronger (see section VB).

VI. Summary

To understand the role of the hydrogen bond accompanied by the vibronic coupling in the formation of X-ray spectra of common molecules, we choose in this paper to study the glyoxalmonoxime molecule in detail. The ground state displays the weakly bound proton-transfer well, which has a higher energy than the global minimum. This makes proton transfer in the ground electronic state practically impossible. However, the ordinary XPS technique is unable to detect the promotion of the proton because the photoionization occurs in a narrow region near the equilibrium. X-ray photoionization visualizes the proton transfer when the molecule is exposed by strong IR pulses. It then gains sufficient energy for intramolecular proton transfer into the weakly bound well of the tautomer 2-nitrosoethenol. The glyoxalmonoxime molecule possess one important feature that makes the studied problem of more general and more fundamental interest: The core-ionization of two inequivalent oxygen atoms results in two qualitatively different potentials that intersect along the proton-transfer coordinate. Due to the crossing of the potentials, the vibronic coupling mixes these states, which implies a partial delocalization, or hopping, of the core hole. So we face interesting dynamics of the wave packets in two vibronically coupled wells that is accompanied by the core-hole hopping. To describe quantitatively the connection of the XPS profile with the dynamics of the system, we developed a corresponding wave packet technique and performed simulations of the X-ray spectra. Calculations show that the vibronic coupling, creating coherent superposition of localized states, influences the spectra even without an IR field. Partial delocalization of the core holes leads to the suppression/enhancement of the newly formed bright/dark core-ionized states. When the molecule is irradiated by a strong IR pulse, two new bands arise in the XPS profile. These bands origin in the core ionization from the region near the weakly bound well of the tautomer 2-nitrosoethenol. The laser induced nuclear wave packet moves in the ground-state well, which makes the intensities of the newly formed XPS bands sensitive to the delay time between the X-ray and the IR pulses.

Our simulation with a Gaussian IR pulse gives a rather delocalized nuclear wave packet. Such a delocalization restricts the spatial resolution of the technique, because one is unable to excite the nuclear subsystem explicitly in a desired point of the proton-transfer coordinate. This strong delocalization origins in the rather poor spectral composition of the wave packet. Thus the shaping of the narrow nuclear wave packet deserves special attention and this is one of the problems suitable for our future efforts.

Acknowledgment. This work was supported by the Conselho Nacional de Desenvolvimento Científico e Tecnológico (CNPq) (Brazil), Swedish Research Council (VR), and Carl Tryggers Stiftelse (CTS) foundation.

References and Notes

(1) Drescher, M.; Hentschel, M.; Klenberger, R.; Ulberacker, M.; Yakovlev, V.; Scrinzl, A.; Westerwalbesloh, Th.; Kleineberg, U.; Heinzmann, U.; Krausz, F. *Nature (London)* **2002**, *419*, 803.

(2) Bressler, C.; Chergui, M. *Chem. Rev.* **2004**, *104*, 1781.

(3) Tschentscher, T. *Chem. Phys.* **2004**, *209*, 271.

(4) Pfeifer, T.; Spielmann, C.; Gerber, G. *Rep. Prog. Phys.* **2006**, *69*, 443.

(5) Svanberg, S. *Atomic and Molecular Spectroscopy*; Springer-Verlag: Berlin, 2001.

(6) Felicíssimo, V. C.; Guimarães, F. F.; Gel'mukhanov, F.; Cesar, A.; Ågren, H. *J. Chem. Phys.* **2005**, *122*, 094319.

(7) Guimarães, F. F.; Kimberg, V.; Felicíssimo, V. C.; Gel'mukhanov, F.; Cesar, A.; Ågren, H. *Phys. Rev. A* **2005**, *71*, 043407.

(8) Guimarães, F. F.; Kimberg, V.; Felicíssimo, V. C.; Gel'mukhanov, F.; Cesar, A.; Ågren, H. *Phys. Rev. A* **2005**, *71*, 012714.

(9) Felicíssimo, V. C.; Guimarães, F. F.; Gel'mukhanov, F. *Phys. Rev. A* **2005**, *72*, 023414.

(10) Köppel, H.; Domcke, W.; Cederbaum, L. S. *Adv. Chem. Phys.* **1984**, *57*, 59.
(11) Gel'mukhanov F.; Ågren, H. *Phys. Rep.* **1999**, *312*, 91.
(12) Ramalingam, M.; Venuvanalingan, P.; Swaminathan, J.; Buemi, G. *J. Mol. Struct.* **2004**, *712*, 175.
(13) Guimarães, F. F.; Kimberg, V.; Gel'mukhanov, F.; Cesar, A.; Ågren, H. *Phys. Rev. A* **2004**, *70*, 062504.
(14) Small, G. J. *J. Chem. Phys.* **1971**, *54*, 3300.
(15) Ballhausen, C. J.; Hansen, A. E. *Annu. Rev. Phys. Chem.* **1972**, *23*, 15.
(16) Kimberg, V.; Guimarães, F. F.; Felicíssimo, V. C.; Gel'mukhanov, F. *Phys. Rev. A* **2006**, *73*, 023409.
(17) Sałek, P.; Gel'mukhanov, F.; Ågren, H. *Phys. Rev. A* **1999**, *59*, 1147.
(18) (a) Becke, A. D. *J. Chem. Phys.* **1993**, *98*, 5648. (b) Lee, C.; Yang, W.; Parr, R. G. *Phys. Rev. B* **1988**, *37*, 785. (c) von Barth, U.; Hedin, L. *J. Phys. C: Solid State* **1972**, *5*, 1629. (d) Becke, A. D. *Phys. Rev. A* **1988**, *38*, 3098. (e) Vosko, S. J.; Wilk, L.; Nusair, M.; *Can. J. Phys.* **1980**, *58*, 1200.
(19) Schmidt, M. W.; Baldridge, K. K.; Boatz, J. A.; Elbert, S. T.; Gordon, M. S.; Jensen, J. H.; Koseki, S.; Matsunaga, N.; Nguyen, K. A.; Su, S.; Windus, T. L.; Dupuis, M.; Montgomery, J. A. *J. Comput. Chem.* **1993**, *14*, 1347.
(20) Krishnan, R.; Binkley, J. S.; Seeger, R.; Pople, J. A. *J. Chem. Phys.* **1980**, *72*, 650.
(21) Guimarães, F. F.; Felicíssimo, V. C.; Kimberg, V.; Cesar, A.; Gelmukhanov, F. *eSP ec Wave Packet Propagation Program*; Universidade Federal de Minas Gerais (Brazil) and Royal Institute of Technology (Sweden), 2004. See http://www.theochem.kth.se/people/freddy/.
(22) Guillemin, R.; Shigemasa, E.; Guen, K. L.; Ceolin, D.; Miron, C.; Leqlercl, N.; Ueda, K.; Morin, P.; Simon, M. *Rev. Sci. Instrum.* **2000**, *71*, 4387.
(23) Ueda, K. *J. Phys. B* **2003**, *36*, R1.
(24) Sugny, D.; Keller, A.; Atabek, O.; Daems, D.; Dion, C. M.; Guerin, S.; Jauslin, H. R. *Phys. Rev. A* **2004**, *69*, 033402.
(25) Szabo, A. *Modern Quantum Chemistry: Introduction to advanced electronic structure theory*; McGraw-Hill: New York, 1989.
(26) Peluso, A.; Santoro, F.; Del Re, G. *Int. J. Quantum Chem.* **1997**, *63*, 233.